Design and fabrication of multi-channel photodetector array monolithic with arrayed waveguide grating*

Qian-Qian Lv(吕倩倩), Pan Pan(潘盼), Han Ye(叶焓), Dong-Dong Yin(尹冬冬), Yu-Bing Wang(王玉冰), Xiao-Hong Yang(杨晓红), and Qin Han(韩勤)†

State Key Laboratory of Integrated Optoelectronics, Institute of Semiconductors, Chinese Academy of Science, Beijing 100083, *China*

(Received 23 July 2015; revised manuscript received 1 December 2015; published online 20 January 2016)

We have provided optical simulations of the evanescently coupled waveguide photodiodes integrated with a 13-channels AWGs. The photodiode could exhibit high internal efficiency by appropriate choice of layers geometry and refractive index. Aseamless joint structure has been designed and fabricated for integrating the output waveguides of AWGs with the evanescently coupled waveguide photodiode array. The highest simulation quantum efficiency could achieve 92% when the matching layer thickness of the PD is 120 nm and the insertion length is 2 μm. The fabricated PD with 320-nm-thick matching layer and 2-μm-length insertion matching layer present a responsivity of 0.87 A/W.

Keywords: photodetector array, monolithic, evanescent coupling, arrayed waveguide grating

PACS: 85.60.Gz, 42.79.Sz, 42.82.Bq **DOI:** 10.1088/1674-1056/25/3/038505

1. Introduction

Due to the increasing demand for speed and capacity of telecommunication systems, dense wavelength-division multiplexing (DWDM) systems with 40 Gb/s channel capacity are widely deployed by major telecommunication carriers to use the existing fiber infrastructure more efficiently.[1] Photonic integrated circuit (PIC) technology optimizes the manufacturing process by choosing InP-based materials, with which it is possible to realize all of the necessary optical functions on a single semiconductor chip.[2] As a multiplexer/demultiplexer, the arrayed waveguide grating (AWG) is the key component in WDM.[3] Photodetectors integrated with AWGs 16×2.5 Gb/s[4] and 10×10 Gb/s[5] have been reported, but the coupling loss is relatively high due to the use of PIN photodiodes.

Evanescently coupled waveguide photodetectors (ECPDs) are key devices in the field of digital, as well as analogue, optical transmissions, due to their high bandwidth and high responsivity.[6–8] This structure permits the efficiency and bandwidth to be specified independently because the internal efficiency is determined not by the thickness but by the length of the photoabsorption layer.[9] The ECPDs can afford high optical coupling efficiency. At the same time, it can achieve higher saturation current than a side-illuminated approach due to more uniform light absorption.[10] Responsivity higher than 1 A/W and bandwidth of 48 GHz have been reported.[11] In addition, their major advantages are the ease of integration with other optoelectronic devices to realize complex systems.[12]

As the epitaxial structure of the evanescently coupled waveguide photodetector[13] and AWGs is quite different, the monolithic configuration has been a design consideration. This letter reports the design concept and numerical simulation results of evanescently coupled photodiodes integrated with AWGs for high quantum efficiency. We optimize the structure of PD and AWGs by choosing appropriate layers' geometry and refractive index. Monolithic integration of photodetector array and AWGs is demonstrated and the device's performance is investigated.

2. Design and simulation

2.1. Design of the integrated structure

The cross section of the AWGs output waveguide is shown in Fig. 1(a), which consists of InP bottom cladding layer, InGaAsP core layer, and InP top cladding layer. The deep ridge waveguide is chosen to achieve a smaller bending radius and polarization independent. The epitaxial structure of the ECPD is different from the AWGs, including a diluted waveguide, a coupled waveguide (InGaAsP), and a p–i–n photodiode with an extended optical matching layer. To integrate AWGs with PD array monotonically, the diluted waveguide and coupling waveguide of ECPD are replaced by the AWG bottom cladding and core layer, respectively, as shown in Fig. 2(a). The epitaxial structure which is realized by the selective area growth (SAG) consists of two areas: the AWG area and PD area. The AWG area includes the top cladding, bottom cladding and core layers, while the PD area includes bottom cladding, core layer, a matching layer, anabsorption layer, and a p-contact layer. Light, initially confined in the AWGs core layer in a single mode, is evanescently coupled to the InGaAs layer due to its higher refractive index. At the

*Project supported by the National High Technology Research and Development Program of China (Grant Nos. 2013AA031401, 2015AA016902, and 2015AA016904), the National Natural Science Foundation of China (Grant Nos. 61176053, 61274069, and 61435002), and the National Basic Research Program of China (Grant Nos. 2012CB933503 and 2013CB932904).

†Corresponding author. E-mail: hanqin@semi.ac.cn

© 2016 Chinese Physical Society and IOP Publishing Ltd

interface, a portion of matching layer with length of L_n is inserted into the AWG cladding layer to enhance the coupling efficiency, thus shortening the detector length to realize higher bandwidth.

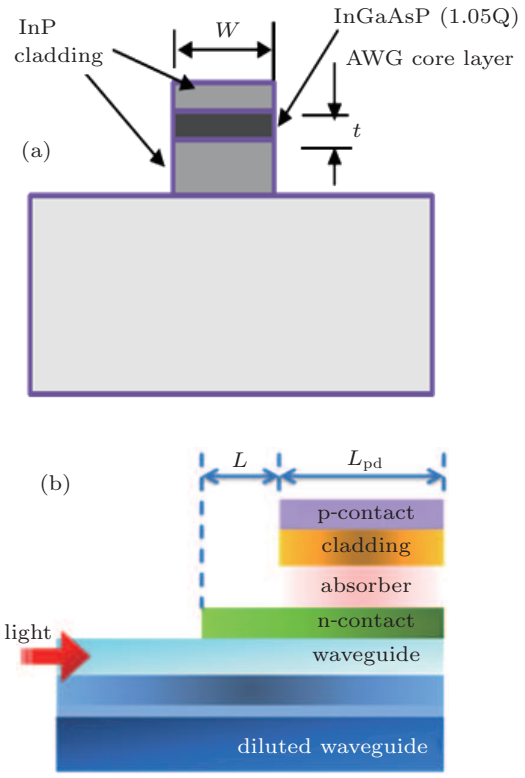


Fig. 1. (a) Cross section of the AWG output waveguide; (b) the lateral section of the ECPD.

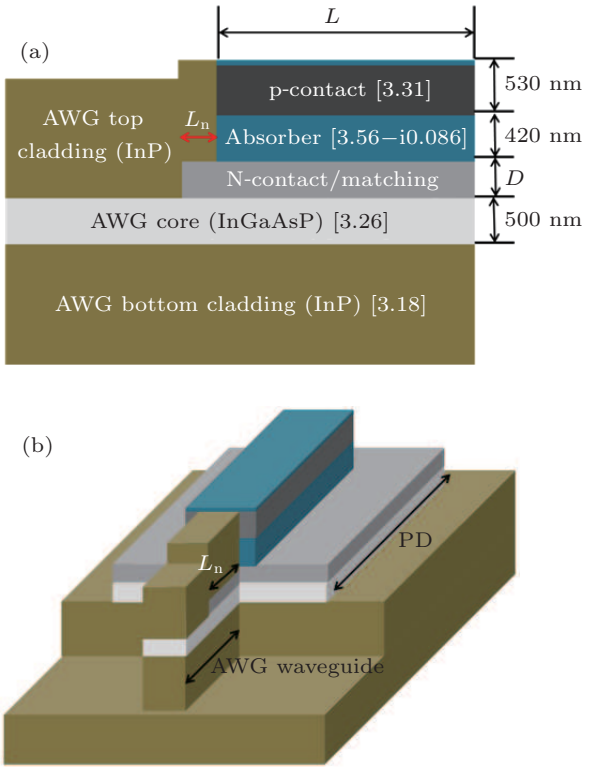


Fig. 2. (a) Cross section of the integrated structure; (b) the schematic structure of the ECPD integrated with the AWG output waveguide.

We design a PD array integrated with 13 output channels of AWGs in a seamless joint structure between the AWG output waveguide and the photodiode, a simple schematic structure as shown in Fig. 2(b). This seamless structure reduces the coupling loss of the AWG and PD.

2.2. Simulations

Simulations of the structure are carried out using 3D finite-difference time-domain (FDTD) solutions. In the FDTD solutions, the optical transmissivity is defined as

$$T(f) = \frac{\int \mathrm{Re}[P(f)^{\mathrm{Monitor}}]\,\mathrm{d}S}{2P_{\mathrm{Source}}}, \tag{1}$$

where $P(f)$ is the Poynting vector and $\mathrm{d}S$ is the surface normal, $T(f)$ is normalized optical transmissivity, which is the ratio of the light power at the simulated cross section and the source power. Thus we can obtain the absorption efficiency by simulating the transmissivity function of the device length.

We suppose the light in the output waveguide of AWGs is a stable single-mode, so the mode source is used and set in the waveguide 10 μm apart from the photodiode. The length of the photodiode is fixed to 40 μm, and the width of the photodiode is fixed to 5 μm. To reach a high bandwidth, we define a 0.42-μm-thick absorption layer. For the optimization of the optical structure, three important parameters are identified: the thickness and refractive index of InGaAsP ($\lambda_g < 1.33$ μm) matching layer above the core layer, the length (L_n) of the matching layer inserted into the AWGs top cladding layer.

The optical matching layer, which also serves as the n-contact layer, provides a refractivity match between the waveguide and the absorption layer to reduce the reflection loss of the refractivity saltation. Therefore, the refractive index affects the optical intensity distribution in the p–i–n photodiode. For a given thickness of the matching layer, we find that light can be rapidly coupled into the absorber with high refractive index of the matching layer as shown in Fig. 3. We can see that the refractive index can change the saturation length of the absorption. To get a higher bandwidth we would reduce the device capacitance by reducing PD length. Thus, the matching-layer refractive index has been set to be a high value of 3.41 to limit InGaAsP compositions to the range of $\lambda_g < 1.33$ μm.

Figure 4 shows the longitudinal electric field distribution of the device without absorption coefficient when the matching-layer refractive indexes are 3.255 and 3.41, respectively. Light confined in the AWG waveguide is a single mode and transfers into the detector at the x coordinate of 100 μm. The light is coupled from the core layer to the matching layer firstly, then transported by periodic concussion of wave type between the absorber and matching layer. This is because that the matching layer can also introduce multimode mode and the

superposition of the multimode mode creates beating effect. The refractive index and thickness of the matching layer will influence the beating effect. When the index is 3.255, there is a weak beating effect as shown in Fig. 4(a). For the index of 3.41 shown in Fig. 4(b) the beating effect is evident, which improves the absorption efficiency of PDs.

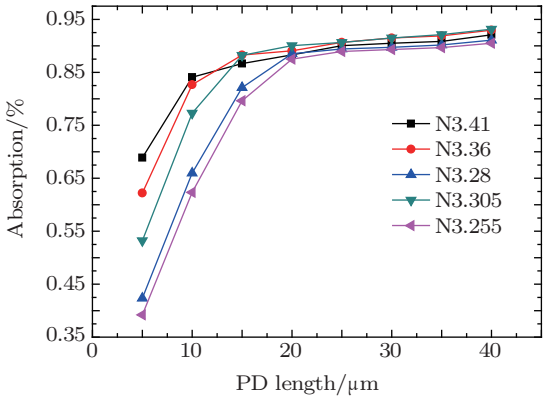


Fig. 3. Absorption efficiency as a function of the device length L with different matching layer refractive indexes.

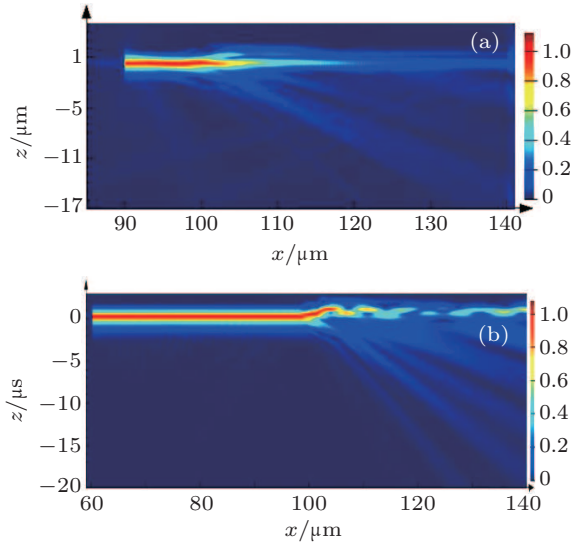


Fig. 4. (a) Longitudinal section of the electric field distribution in device without absorption coefficient when the refractive index of matching layer is 3.255; (b) the longitudinal section of the electric field distribution in device without absorption coefficient when the refractive index of matching layer is 3.41.

The thickness is another factor to beating effect. For the seamless structure, changing the matching-layer thickness, then the optimized matching layer thickness will be determined and the simulated result is shown in Fig. 5. The best performance corresponds to a photodiode with a matching layer thickness of 120 nm and the internal quantum efficiency is as high as 92%. Due to the matching layer that also acts as the n-contact layer, thicker matching layer ($D = 220$ nm or $D = 320$ nm) could be selected to obtain a smaller lateral resistance, which exhibits quasi-optimal absorption (still $> 85\%$).

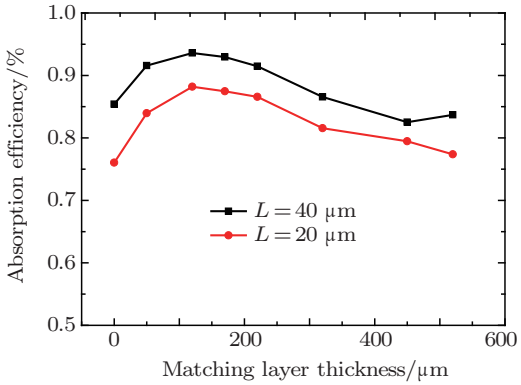


Fig. 5. Absorption efficiency as a function of matching layer thickness D with different device length L.

At the interface, in order to enhance the coupling efficiency, a portion of matching layer with length of L_n is inserted into the AWG cladding layer. The L_n influences the electric field distribution at the absorber interface due to the beating effect. The influence of the matching layer insertion length L_n and the optical characteristic of this structure is studied. The typical simulation results of the absorption efficiency versus the matching layer insertion length L_n are presented in Fig. 6, from which one can confirm that for a fixed value of matching layer thickness, the absorption efficiency with a shorter device length (L_{pd}) is more sensitive to L_n. Taking the case of $D = 320$ nm and $L_{pd} = 10$ μm for example, the absorption efficiency is enhanced by more than 10% compared to $L_n = 0$. In order to achieve a higher bandwidth than 60 GHz, the device length could decrease to 10 μm, in which the absorption efficiency will strongly depend on the L_n. It corresponds to optimal absorption of 80% and 76% under the optimum $L_n = 4$ μm and $L_n = 2$ μm, for $D = 220$ nm and $D = 320$ nm, respectively.

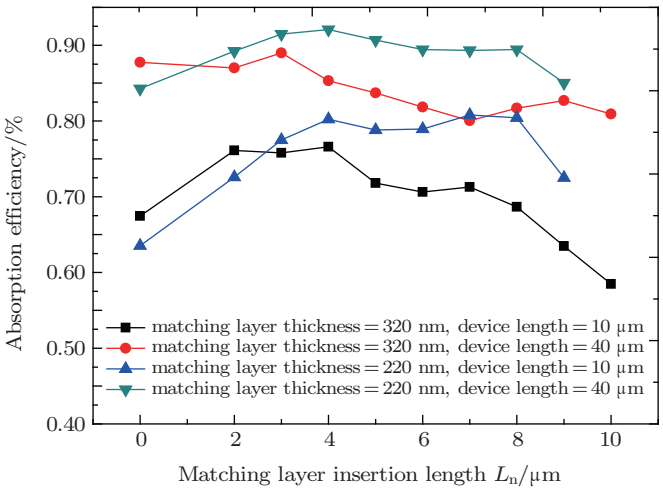


Fig. 6. Absorption efficiency as a function of insertion length L_n with different device length L and matching layer thickness D.

3. Fabrication and results

After obtaining these simulation results, the epitaxial structure with optimized parameters was grown using the metalorganic chemical vapour deposition (MOCVD) technique

on an InP semi-insulating substrate. For the seamless structure, the first epitaxial structure consists of an AWG bottom cladding layer, core layer, and the p–i–n structure as shown in Table 1. The epitaxial structure of the PD compatible with the AWGs is realized by utilizing the selective area growth (SAG). Firstly, a 500-nm-thick SiO_2 was deposited on the wafer. After that we use the inductively coupled plasma (ICP) and selective wet etching (H_2SO_4:H_2O_2:H_2O) to remove the p–i–n structure of the AWG area. Then the AWG top cladding layer was regrown at the AWG area by MOCVD, while the PD area was covered with SiO_2 without regrowth.

Table 1. The first epitaxial structure of the integrated device.

Function	Compound	*D*/nm	Dopant	N/cm^{-3}
p-contact	$In_{0.53}Ga_{0.47}As$	80	Zn	1.0×10^{19}
grading	$InGa_{0.3}As_{0.64}P$	5	Zn	5.0×10^{18}
cladding	$InGa_{0.18}As_{0.39}P$	410	Zn	1.0×10^{18}
spacer	$InGa_{0.18}As_{0.39}P$	30	Zn	5.0×10^{17}
grading	$InGa_{0.34}As_{0.73}P$	5	Zn	1.0×10^{17}
absorption	$In_{0.53}Ga_{0.47}As$	420		
etch stop1	InP	10		
n-contact	$InGa_{0.3}As_{0.64}P$	320	Si	2.0×10^{18}
etch stop2	InP	10		
AWG core	$InGa_{0.11}As_{0.25}P$	500		
AWG bottom	InP	1000		
substrate	InP	50000		

The results of the regrowth epitaxial structure are shown in Fig. 7. We can see there is an abnormal growth at the interface in SAG as shown in Figs. 7(a) and 7(b), which will bring adverse effects to device fabrication. The abnormal growth is sensitive to the crystal orientation and could be suppressed by choosing the [0 −1 1] orientation as shown in Fig. 7(b), with a better surface at the interface. The regrowth top cladding layer is intrinsic, which insures the isolation of the two device structures.

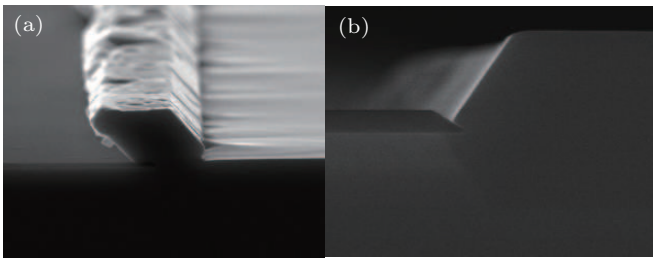


Fig. 7. The scanning electron micrograph (SEM) images of the regrowth structure: (a) the epitaxial structure by SAG in [011] orientation; (b) the epitaxial structure by SAG in [0 −1 1] orientation.

Device fabrication is carried out using conventional lithography techniques and standard InP processing techniques. Firstly, the p mesa was etched down to the n-contact layer with a sequence of wet etching and inductively coupled plasma (ICP) etching. Secondly, the larger *n* mesa was etched down into the un-doped waveguide layer. Thirdly, the device was passivated and the contact metals deposited. Finally, an SiO_2 layer was grown by plasma enhanced chemical vapor deposition (PECVD) as a hard mask and AWGs structure was formed by a lithography step and inductively coupled plasma (ICP) etching.

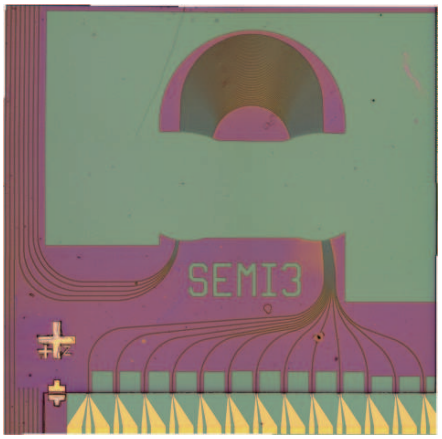


Fig. 8. Microscopeimage of the fabricated ECPD array integrated with a 13-channel AWG.

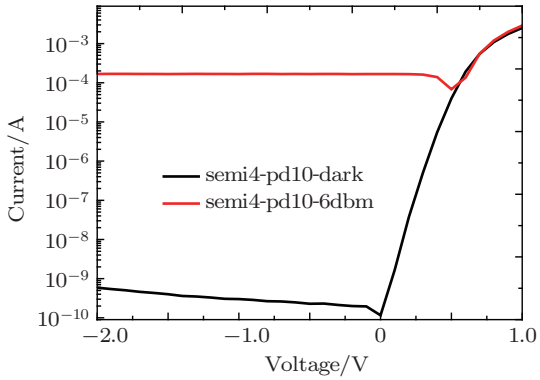


Fig. 9. The measured current as a function of the bias voltage with seamless structure.

Figure 8 shows the seamless joint PDs with 320-nm-thick matching layer integrated with AWGs. The photoresponse measurement is carried out using a semiconductor parameter meter and a tunable laser at C band. As shown in Fig. 9, the photocurrent of the integrated device can achieve 187 μA when the laser power is 6 dBm. The measured total coupling efficiency is −13.3 dB, which includes an AWGs on-chip loss, the coupling loss between input waveguide and the tapering fiber, the coupling loss from the AWG output waveguide to the photodiode. The measured response of the AWGs without regrowth is about −9 dBm and the measured response of the straight waveguide is −4 dBm, when the source is 5.3 dBm as shown in Fig. 10. The single-ended coupling efficiency is about −4.6 dB, calculated using the straight waveguide response. Hence, the coupling efficiency from the fiber to the AWG output waveguide is about −9.7 dB. Moreover, after the second epitaxial growth and photodiode technological process,

the best measured AWG response would decrease about 3 dB. Then the coupling efficiency from the AWG output waveguide to the photodiode is about −0.6 dB, which correspond to 0.87 A/W. The result is in agreement with the absorption efficiency of 85% (1 A/W) in the FDTD simulations.

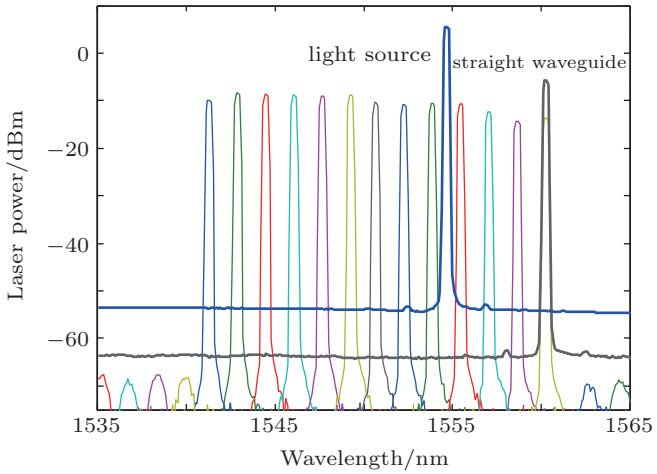


Fig. 10. The spectral response of the fabricated AWG without regrowth.

4. Conclusion

In this letter, we have designed and optimized the epitaxial structures of evanescently coupled photodiodes integrated with AWGs. A higher absorption efficiency of 85% is achieved by seamless joint between the AWG and PDs, in which the thickness of matching layer is 320 nm and the insertion length is 2 μm. The experiment result is 0.87 A/W, which is consistent with the simulation results. According to the theoretical calculation, the individual devices could realize a bandwidth more than 10 GHz, which are integrated with a 10-channels AWGs and can reach a high capacity of 100 Gb/s.

References

[1] Bottacchi S, Beling A, Matiss A, Nielsen M L, Steffan A G, Unterbörsch G and Umbach A 2010 *IEEE J. Select. Topics Quantum Electron.* **16** 1099
[2] Coldren L A, Nicholes S C, Johansson L, Ristic S, Guzzon R S, Norberg E J and Krishnamachari U 2011 *J. Lightw. Technol.* **29** 554
[3] Pan P, An J M, Wang H J, Wang Y, Zhang J S, Wang L L, Dai H Q, Zhang X G, Wu Y D and Hu X W 2014 *Chin. Phys. B* **23** 044210
[4] Yoshikuni Y 2002 *IEEE J. Select. Topics Quantum Electron.* **8** 1102
[5] Nagarajan R, Joyner C H, Schneider R P, *et al.* 2005 *IEEE J. Select. Topics Quantum Electron.* **11** 50
[6] Beling A and Campbell J C 2009 *J. Lightw. Technol.* **27** 343
[7] Zhang Y, Zuo Y H, Guo J C, Ding W C, Cheng B W, Yu J Z and Wang Q M 2009 *Chin. Phys. B* **18** 225
[8] Bach H G, Beling A, Mekonnen G G, Kunkel R, Schmidt D, Ebert W, Seeger A, Stollberg M and Schlaak W 2004 *IEEE J. Select. Topics Quantum Electron.* **10** 668
[9] Park J W 2010 *IEEE Photon. Technol. Lett.* **22** 975
[10] Takeuchi T, Nakata T, Makita K and Yamaguchi M 2000 *Electron. Lett.* **36** 972
[11] Demiguel S, Li N, Li X W, Zheng X G, Kim J, Campbell J C, Lu H F and Anselm A 2003 *IEEE Photon. Technol. Lett.* **15** 1761
[12] Ghirardi F, Bruno A, Mersali B, Brandon J, Giraudet L, Scavennec A and Carenco A 1995 *J. Lightw. Technol.* **13** 1536
[13] Liu S Q, Yang X H, Liu Y, Li B and Han Q 2013 *Chin. Phys. B* **22** 108503